promoting access to White Rose research papers

Universities of Leeds, Sheffield and York
http://eprints.whiterose.ac.uk/

This is an author produced version of a paper published in **Proceedings of the 6th MIRA International Vehicle Aerodynamics Conference.**

White Rose Research Online URL for this paper:
http://eprints.whiterose.ac.uk/3770/

Published paper
Gilkeson, C.A., Wilson, M.C.T., Thompson, H.M., Gaskell, P.H., Barnard, R.H., Hackett, K.C. and Stewart, D.H. (2006) *Ventilation of small livestock trailers.* In: 6th MIRA International Vehicle Aerodynamics Conference : Real World Aerodynamics. The 6th MIRA International Vehicle Aerodynamics Conference, 25th -26th October 2006. MIRA .

White Rose Research Online
eprints@whiterose.ac.uk

Ventilation of Small Livestock Trailers

C.A. Gilkeson, M.C.T. Wilson, H.M. Thompson, P.H. Gaskell,
R.H. Barnard*, K.C. Hackett, and D.H. Stewart****
The University of Leeds, School of Mechanical Engineering
*The University of Hertfordshire
**Qinetiq Ltd

ABSTRACT

A large number of livestock is transported to market in small box trailers. The welfare of animals transported in this way is now assuming greater importance with the onset of tougher EU legislation. This paper presents the first study into the ventilation of small livestock trailers using experimental and computational methods. Wind tunnel studies, using a $1/7^{th}$ scale model, highlight the important influence of the towing vehicle and trailer design on the airflow within the trailer. Detailed CFD analysis agrees well with the wind tunnel data and offers the ability to assess the impact of design changes.

INTRODUCTION

The movement of livestock from farms to market is an essential part of the agricultural industry. Effective control of the thermal micro-climate within a transport vehicle can improve animal welfare. Though there are no previous studies of ventilation in small box trailers, larger-scale vehicles have been analysed. For example, the external pressure field around a moving poultry transporter has been shown to dictate the internal airflow patterns, whereby the internal flow naturally opposes vehicle movement [1]. Air tends to enter the rear of the container, move forward over the animals and exit through front grilles. Separation regions around the front of the vehicle aid the extraction of airflow (suction) through these grilles. Further investigation resulted in the development of an actively controlled ventilation system for large livestock transport vehicles [2]. The low pressures existing in the front separation regions were exploited using actively controlled fans. The fans were designed to aid suction through the front grilles and maintain a constant flow over the animals. Trials found that the ventilation system successfully removed significant amounts of heat and moisture generated by the animals during transit.

Despite their high level of use, the ventilation characteristics of smaller livestock trailers have largely been overlooked. A leading livestock trailer manufacturer estimates that around 60,000 of their vehicles are currently in use within the UK today [3]. Box trailers of this type rely on passive ventilation alone and little is known about how the design and movement of the trailer and towing vehicle affect the internal environment. Ultimately the goal of this study is to assess the performance of such passive ventilation in trailers by accounting for heat generation by the livestock as well as solar radiation. This paper describes the first stage of the investigation, namely an isothermal study of the airflow during steady forward movement of the empty vehicle, which is used to validate CFD models against wind tunnel tests.

EXPERIMENTAL PROCEDURE

Wind tunnel tests were carried out on a 1/7th scale model at the University of Hertfordshire. The model consisted of a livestock trailer and a generic towing vehicle angled at zero degrees to the oncoming flow, see Figure 1. Two vehicle configurations were considered, namely the coupled case with both the towing vehicle and the trailer, and the trailer-only case. The latter case was tested as an extreme example of using a streamlined towing vehicle, whereby a large proportion of the front of the trailer would be exposed to the advancing airflow. The trailer itself was split into two separate decks and each had a series of rectangular vents down either side, resulting in eight vents per side, see Figure 2. A large rear vent spanning the width of the trailer was also present on the top deck, this being representative of current livestock trailer design.

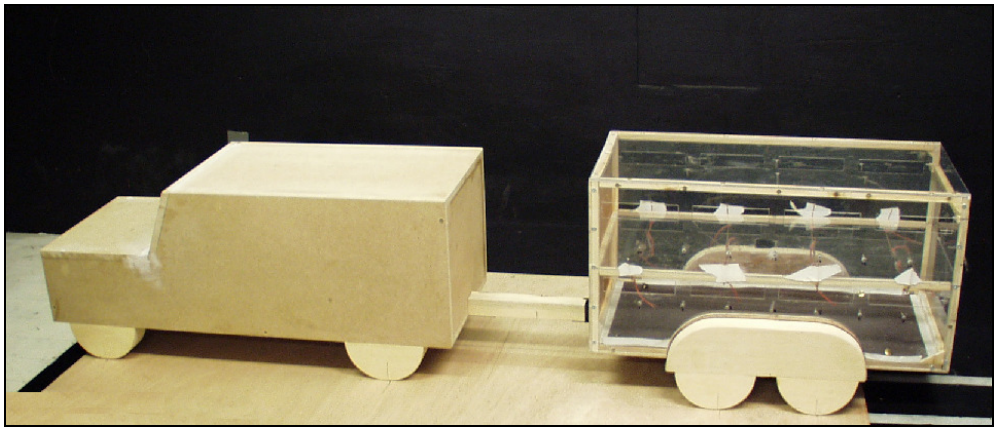

Figure 1 – Side view of the model livestock trailer and towing vehicle.

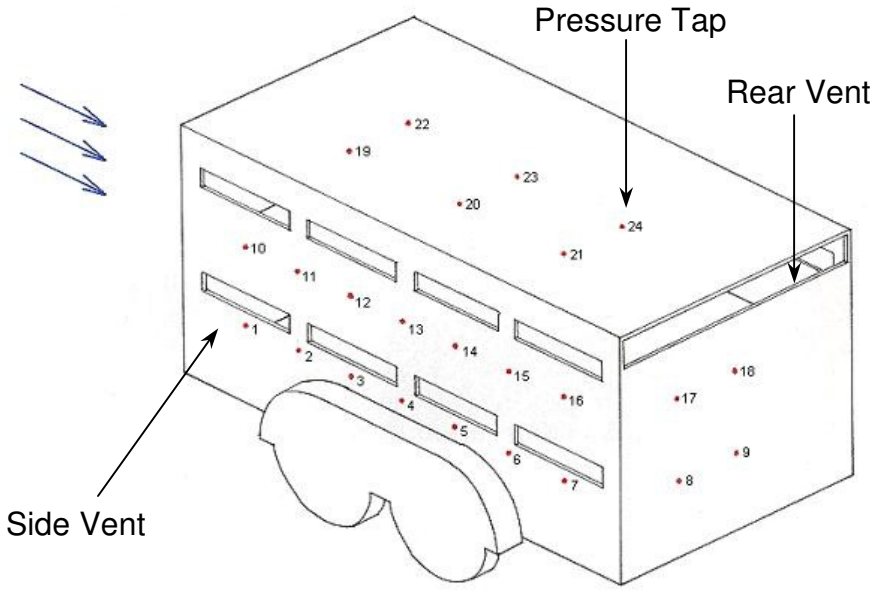

Figure 2 – Isometric view of the model trailer with numbered pressure tap locations.

A total of twenty-four pressure taps were evenly distributed along the nearside of the trailer and connected to a multi-channel Sensor Technics pressure transducer. Velocity measurements were made using a coupled pair of small pitot and static tubes, as a simple yet effective means of measuring normal velocities through the vent apertures. A series of metal hangers housing wool tufts were made to provide a qualitative understanding of the flow structure inside the trailer. The small scale of the model did not justify implementing a moving ground plane and so a ground board was used instead. This strategy raised the model above the boundary layer of the wind tunnel floor to minimise unrealistic ground effects.

The working section of the open-return wind tunnel tapered from 1.540m x 1.223m on entry to 1.582m x 1.282m on exit. The resulting blockage imposed on the airflow by the model was only 3.42%. With the wind tunnel in operation, a free-stream air velocity of 19.7 m/s passed over the model. With a characteristic vehicle length of 1.357m for the coupled vehicle case, the Reynolds number was found to be 1.8×10^6. The experimental procedure consisted of calculating pressure coefficients at the prescribed locations, based on the free-stream dynamic pressure measured using a pitot-static tube aligned above the cab of the towing vehicle and well clear of the local flow effects. Each pressure measurement was made with a sampling frequency of 100Hz and time averaged over 20 seconds. The air velocities were measured normal to the vent apertures on the left hand side of the vehicle and across the span of the rear vent. The tests were concluded with photographic analysis of the movement of the wool tufts during a flow visualisation exercise.

COMPUTATIONAL MODELLING

The commercial CFD code used for the numerical simulations was Fluent 6.2.16 and the computational grid produced in Gambit [4]. Two computational models were created, one for each of the configurations tested. Both solution domains matched the internal dimensions of the wind tunnel, including the contracted intake, the ground board and the tapered working section. A 20m rectangular duct was added to the front of the wind tunnel to provide a more realistic inlet boundary condition, since no information on the velocity distribution entering the tunnel was available. The symmetrical nature of the domain permitted use of a symmetry plane along the centreline of the model. A velocity inlet and a pressure outlet were used as respective boundary conditions at either end of the domain.

The solution domain was decomposed into various boxes including a central volume, which encompassed the model vehicles and the ground board. A hybrid mesh was composed with unstructured cells within the central volume and structured cells throughout the rest of the domain. A preliminary study into grid independence was used in order to select the optimum number of cells for the primary study. This was achieved by refining the mesh density within the central volume only, allowing the structured cells to remain unchanged. A series of eight grids were created with the global number of cells ranging from 0.8 – 3.5 million, the finest of which is shown in Figure 3.

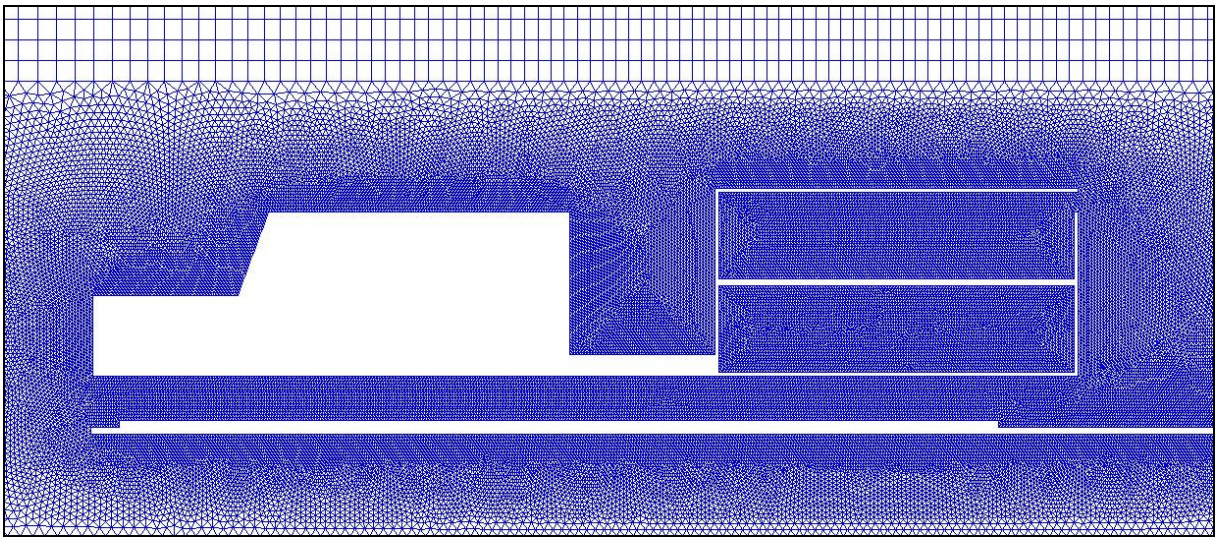

Figure 3 – A cross-section of the finest computational grid for the two-vehicle configuration.

Isothermal second order steady state simulations were conducted for each grid using three turbulence models. Solutions for the free-stream velocity and the model drag coefficient were computed using the Spalart-Allmaras (SA) model [6], the standard *k-ε* model [7] and the Reynolds Stress Model (RSM), see Figure 4.

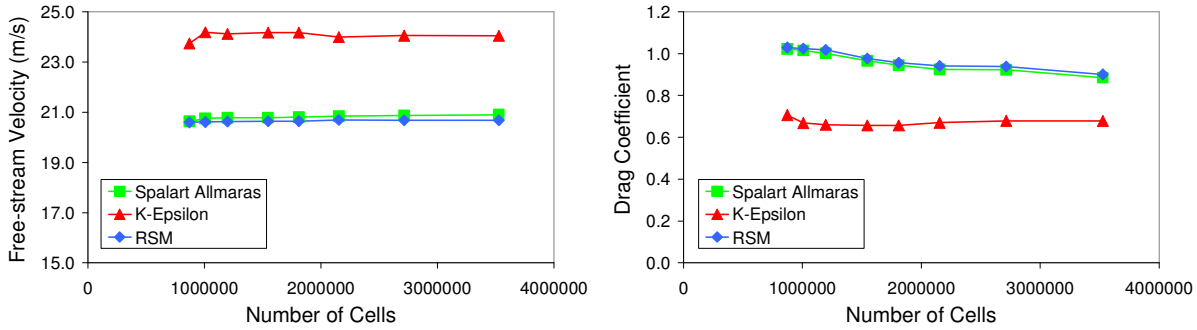

Figure 4 – Results from the grid independence study for the two-vehicle case.

General solution convergence was seen for all three turbulence models as the number of cells increased. Free-stream velocities were almost constant as the density of the grid increased from 2 to 3.5 millions cells. Solution convergence for the drag coefficient was equally as pronounced using the *k-ε* model, although some grid dependency was evident for the other two models. Despite this grid dependency, the number of cells generated in grid number 8 was the maximum possible with the computational resources available. In order to better quantify the error between the fine grid and the asymptotic solution for zero grid spacing, Richardson extrapolation [8] was applied to the finest and coarsest grids, taking solution quantities and grid spacing into account, see Table 1. The errors predicted in the free-stream velocity measurements were less than 2% for the Reynolds Stress Model with a 6% error for the Spalart Allmaras model and the worst performer was the *k-ε* model, with an error

estimate of over 7%. Errors in the drag coefficient predictions were less than 4% for all three models.

Grid	U_∞			C_D		
Number	SA	k-ε	RSM	SA	k-ε	RSM
1 (Coarse)	20.637	23.737	20.598	1.023	0.707	1.030
8 (Fine)	20.901	24.047	20.682	0.886	0.679	0.901
Error	-6.25%	7.33%	1.99%	-3.24%	-0.66%	-3.05%

Table 1 – Solution errors for the three turbulence models used.

Results from the preliminary study were also used to highlight the best performing turbulence model, in spite of the predicted errors. All three were implemented with standard wall functions due to the limited number of cells imposed by the grid. Wall y^+ values on the vehicle surfaces were in the recommended range of 30 – 50 [9]. Implementing enhanced wall treatment would have involved using a prohibitively large number of cells. Static pressure coefficients were computed for each turbulence model along the bottom line of pressure taps on the side of the livestock trailer and compared against the experimental pressures, see Figure 5.

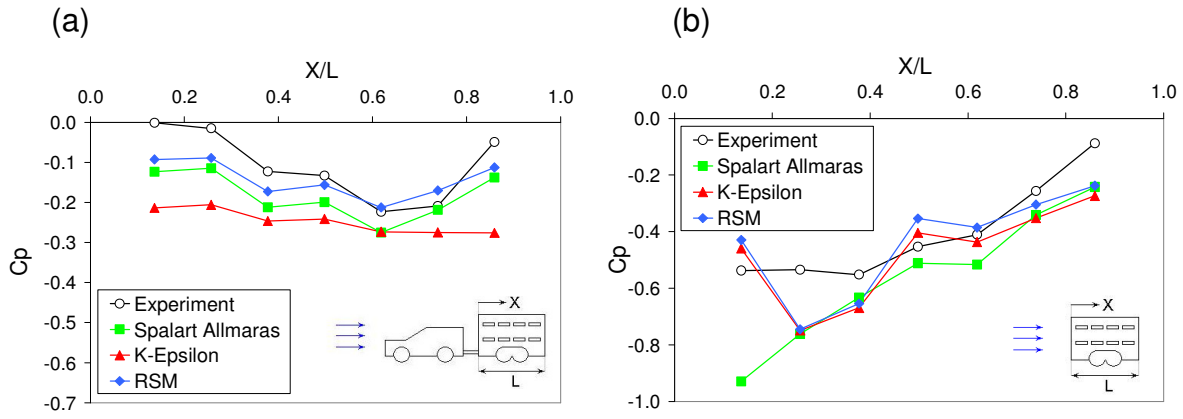

Figure 5 – Lower side pressure profiles computed using three turbulence models for (a) the coupled vehicle case and (b) the trailer-only case.

For the coupled vehicle case, the one-equation Spalart-Allmaras model predicted a pressure distribution with the best gradient between data points, see Figure 5(a). The same trend was seen for the trailer-only case, see Figure 5(b). In addition, solution convergence was obtained with ease using the Spalart-Allmaras model whereas the RSM model in particular showed great instability and required excessive over relaxation. The poorer match between experimental and computational results using the *k-ε* model, allied with the largest errors highlighted above were cited as reasons not to use this model during the primary study. A decision was thus taken to compare the Spalart-Allmaras model with the experimental results for the entire data set.

RESULTS

Quantitative results from both the experimental and computational procedures are presented in Figures 6 – 8. The experimental pressures were averaged over three runs for both vehicle configurations.

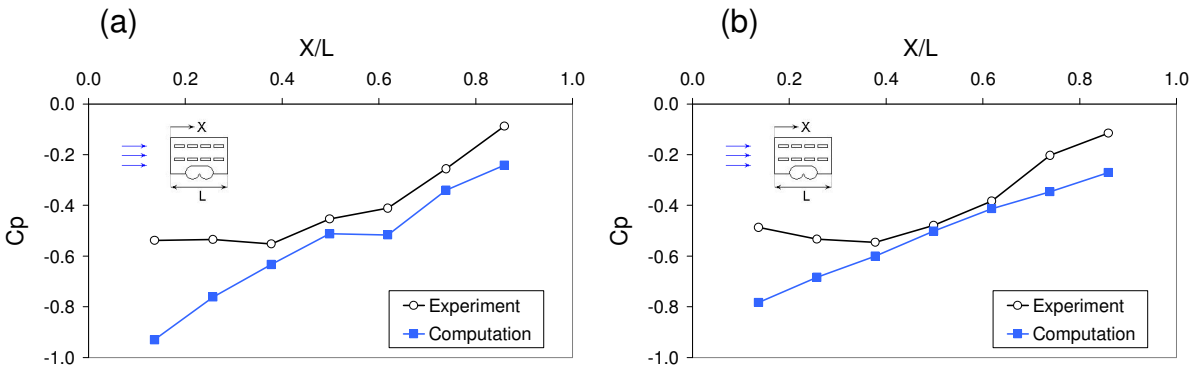

Figure 6 – Side pressure distribution adjacent to (a) the lower vents and (b) the upper vents for the livestock trailer only.

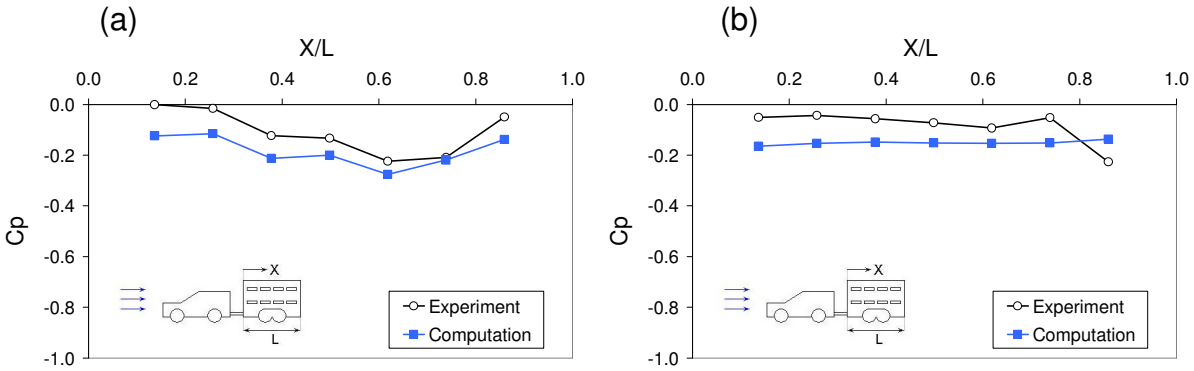

Figure 7 – Side pressure distribution adjacent to (a) the lower vents and (b) the upper vents for both vehicles.

Observing the trailer-only case, experimental pressure distributions showed a low-pressure separation region at the front of the trailer, with pressures relaxing close to ambient conditions towards the rear, see Figure 6. The same trend was evident for pressures measured adjacent to the lower and upper vent stations respectively. The CFD model predicted the same general flow structure, with abrupt separation around the front of the trailer and subsequent reattachment at the rear. However, the computational results do predict larger separation regions with pressure coefficients over-predicted by a factor of almost two. From about one-third distance along the side of the trailer, the computational results correspond with the experiments and the pressure gradients are accurately reproduced.

For the more realistic two-vehicle case, both techniques exhibited partially attached airflow along the sides of the trailer, see Figure 7. Moderate separation occurred along the lower vent stations due to the close proximity of large wheel arches,

however the pressures relaxed towards the rear. Once again, the computational results produced larger pressure coefficients but the pressure gradients were very similar along the entire length of the vehicle. The magnitudes of the pressure coefficients were significantly lower than those shown for trailer-only configuration.

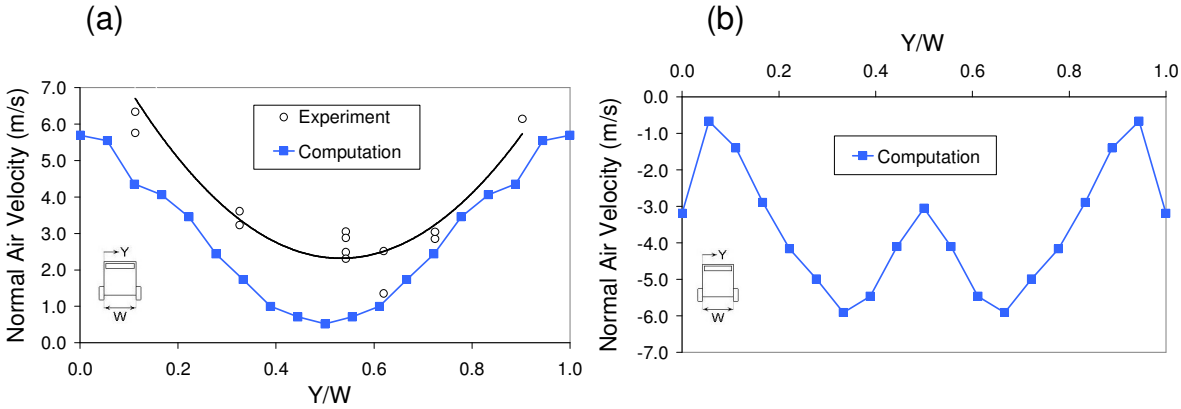

Figure 8 – Velocity distribution normal to the rear vent for (a) both vehicles and (b) the trailer only.

The velocity distribution across the rear vent was found to be parabolic in nature for the coupled vehicle case, see Figure 8(a). Both the experimental and computational results predicted elevated velocities of approximately 6m/s at either side of the vent. This result also highlighted slower moving airflow in the centre of the vent, indicating that the internal air currents were relatively slow, with respect to the free stream. Measuring the rear vent velocities using the velocity probe for the trailer-only yielded null readings. This result occurs when the pitot tube reads a smaller value than the static tube, hence the velocity probe was incapable of measuring negative velocities. The computational model verified that the air currents were in fact opposing the free air stream and *entering* the rear vent. The fastest velocities were found to be 6m/s occurring near to the centre of the vent, signifying a faster internal flow regime, see Figure 8(b).

The flow visualisation technique allied with the velocity and pressure data was used to construct a general flow diagram through each of the two vent planes for both vehicle configurations. For the trailer-only case, the flow field on the upper and lower decks were very similar with the exception of airflow entering the rear vent on the upper deck, see Figures 9(a) and (b). The oncoming airflow tended to strike the front face of the trailer and spill around the sides, before entering the rearmost side vents, mixing with the internal air volume and exiting through the front vents. The computational model also predicted this circuit of airflow. Contour plots of velocity magnitude highlight fast normal velocity components extending into the trailer through the rear side vents, and out of the front vents, see Figures 9(c) and (d). The CFD results also emphasize the extent of slow moving air behind the front face of the trailer. Particles released from the side and rear vent openings highlighted the unsteady nature of the flow, see Figure 10. The flow field is highly three-dimensional with a complex structure exhibiting significant levels of vorticity. Large quantities of air can be seen exiting the trailer with a strong migration towards the roof of the vehicle.

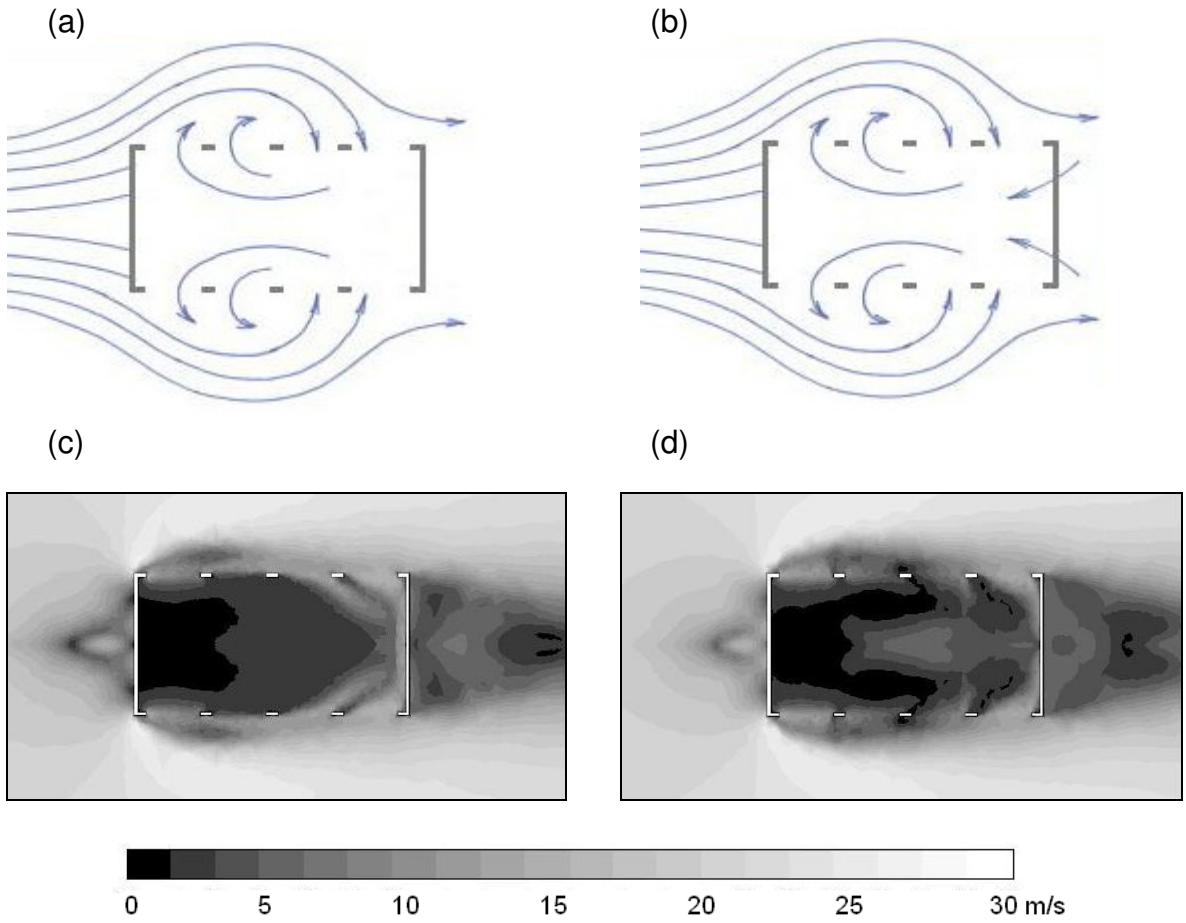

Figure 9 – Flow visualisation for the trailer-only case: Experimental flow field for (a) the lower deck and (b) the upper deck, computational velocity magnitudes for (c) the lower deck and (d) the upper deck, free-stream velocity 20m/s.

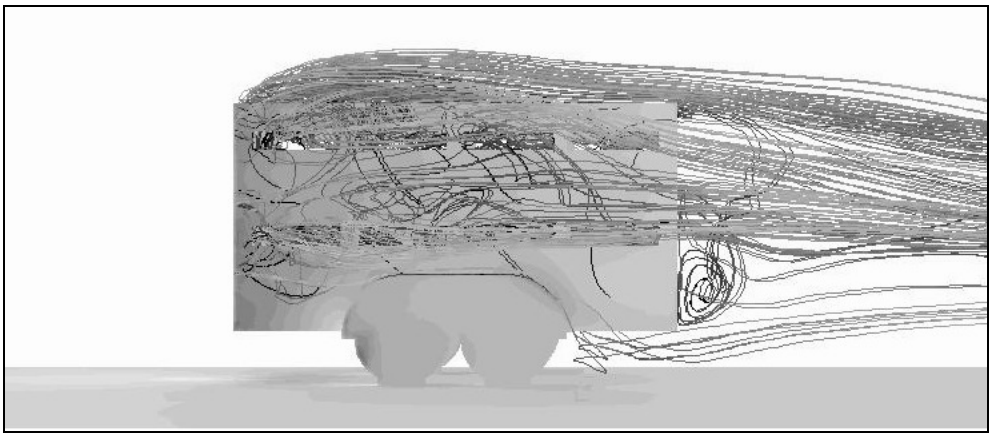

Figure 10 – Side view of path lines for particles released from all seventeen vents overlaying a surface contour plot of static pressure, trailer-only.

The flow field for the coupled vehicle case is shown in Figure 11. In contrast to the trailer-only configuration, differing internal airflow patterns occurred on each deck. It was shown that very little mixing occurs within the lower deck, with the majority of external airflow tending to skip past the trailer, see Figures 11(a) and (c). On the upper deck, the external flow entered the three rearmost vent stations with velocities comparable to the free stream, before exiting through the rear vent, see Figures 11(b) and (d). Again, regions of low air velocity were identified behind the front face of the trailer but they were more widespread than for the isolated trailer arrangement. The absence of low-pressure separation regions to extract air from the front vent apertures is likely to account for this.

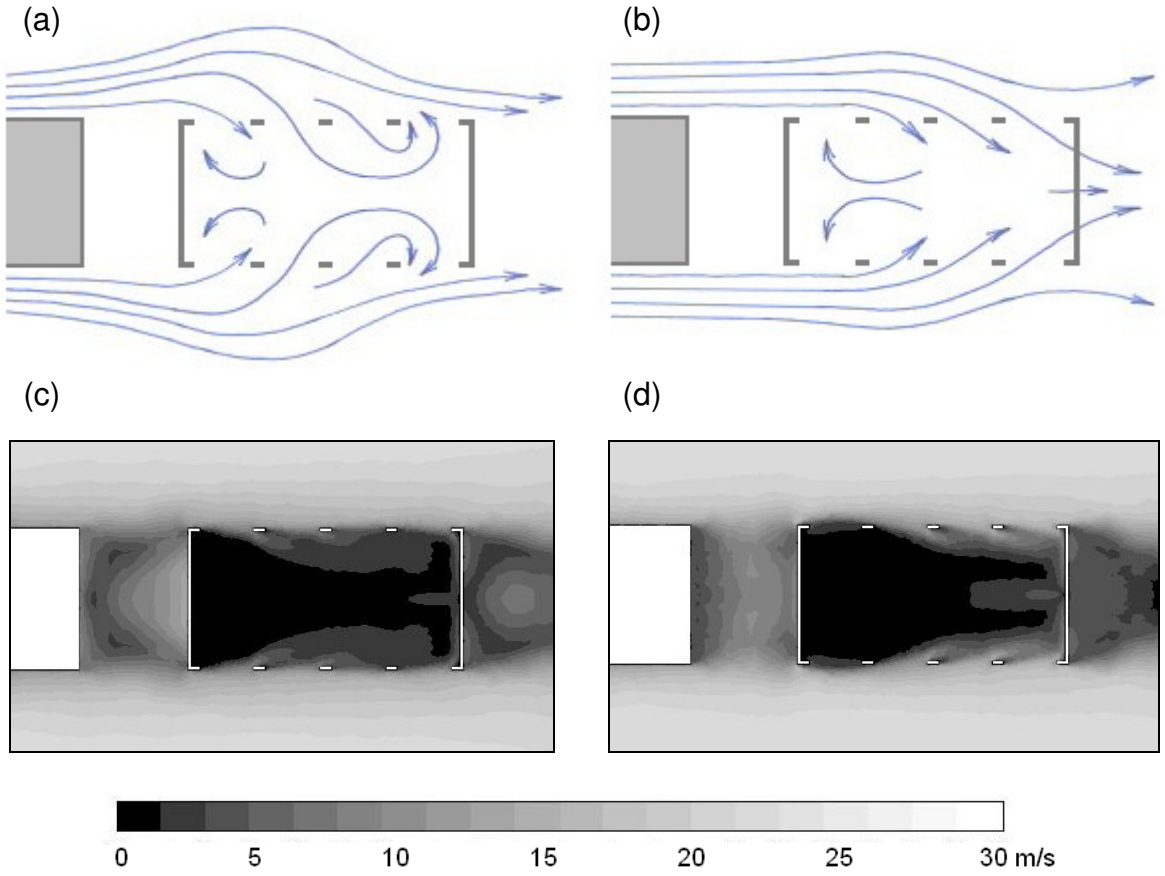

Figure 11 – Flow visualisation for the two-vehicle case: Experimental flow field for (a) the lower deck and (b) the upper deck, computational velocity magnitudes for (c) the lower deck and (d) the upper deck, free stream velocity 20m/s.

The steady, structured nature of the airflow with the towing vehicle present is shown in Figure 12. Most of the air entering the side vents on the upper deck is clearly seen exiting the rear vent. In contrast to the trailer-only configuration, a small proportion of the internal air volume appears to be exiting the trailer, with some spillage from the rearmost lower side vents only.

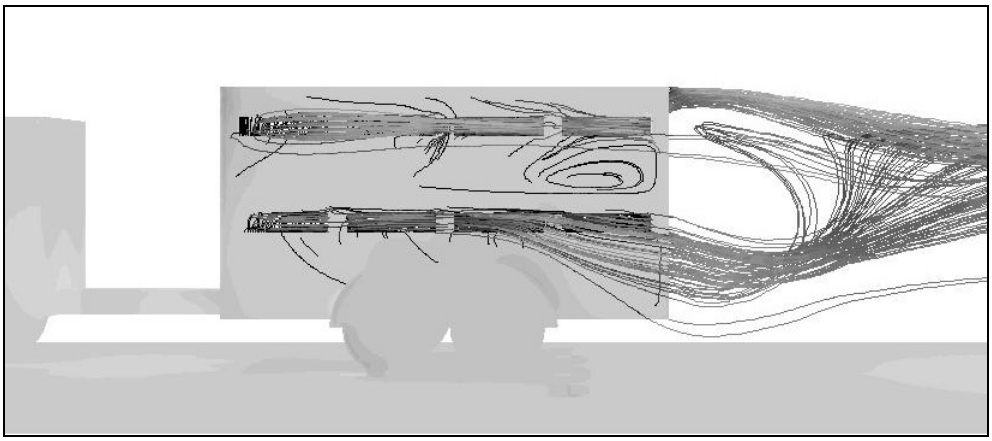

Figure 12 – Side view of path lines for particles released from all seventeen vents overlaying a contour plot of static pressure, both vehicles.

Since the scale of the model was relatively small, the observed free-stream velocity of approximately 20m/s only represented a full-scale speed of 2.8m/s (keeping the Reynolds number constant). Typical operating speeds for livestock trailers are in the range of 15-25m/s and so it was necessary to run some CFD simulations using elevated velocities to check the whether the topology of the flow structure changed. Inlet velocities were increased such that the free-stream velocity reached 102m/s, producing a Mach number of 0.3, which was considered to be on the limit of incompressibility. This represented a full-scale velocity of 15m/s. For the trailer-only case, the flow structure was largely the same with separation dominating the external flow and extensive regions of slow-moving air inside the trailer, as before. Results for the coupled case showed that more air from the free-stream entered the upper deck of the trailer and this reduced the size of the low velocity region behind the front face, however the same features were still present. The only significant change in the flow structure was an additional region of slow-moving air, occurring on the lower deck ahead of the tailgate.

DISCUSSION

The results from the experimental and computational methods enabled a detailed picture of the flow field surrounding a typical livestock trailer to be assembled. The CFD models complemented the wind tunnel data and good agreement between the two techniques was found, both in terms of the measured quantities and qualitative aspects of the flow. Results for the trailer-only case were dominated by a large separation around the front face of the trailer. This result is to be expected due the adverse pressure gradients caused by the sharp corners of the trailer. Low pressures in these regions tended to extract air from the trailer through the front vent stations on both decks, whilst drawing air in through the rear vent on the upper deck. Moving towards the rear of the vehicle, external flow reattached to the sides allowing air to enter the rear vent stations. The net effect of the external flow structure was to induce a circuit of airflow, which appears to continuously exit and re-enter the trailer. Despite the fact that the internal air velocities were actually higher in this case, intuition

suggests that any outflow from the trailer is likely to be re-ingested, so it may not be very effective in terms of ventilation. Clearly, livestock trailers cannot be used without some form of towing vehicle and so this situation is very unlikely to occur. However, the results do suggest that if a smaller or more streamlined vehicle were to be used, ventilation could be adversely affected.

Of all the results obtained, emphasis was on the more realistic coupled vehicle scenario. The external flow was largely attached, with the exception of some moderate wheel arch induced separation in the vicinity of the central lower vent apertures. It is likely that the advancing airflow separated around the front of the towing vehicle due to its blunt shape, before reattaching at some point downstream. Attached flow was maintained across the towing gap and along the sides of the trailer. The external air stream duly entered the upper side vents and exited the rear vent above the tailgate. The low-pressure wake behind the rear face of the trailer is likely to have driven the flow through the upper deck in the fashion observed. The absence of a rearward-facing vent on the lower deck prevented the low-pressure wake from interacting with the internal flow, thus preventing air from being pulled through the cabin. As a result, the external flow tended to skip past the lower side vents with significantly less air flowing inside the trailer. However, the flow structure around the trailer as a whole was much more structured than for the trailer-only case.

The reliability of the wind tunnel velocity measurements normal to the side vents was brought into question during results analysis. The actual flow direction was quite oblique to the side apertures and so accurately measuring the normal velocity component was unattainable with the probe used. The only way to measure the flow with any degree of accuracy would have been to use a three-component hot wire anemometer, however this was beyond the scope of the present study. It was for these reasons that the velocities predicted by the CFD models were relied upon in the analysis of the flow fields, and the general agreement with other experimental quantities (namely pressure) justified this approach.

Velocity magnitude contour plots obtained from the CFD analysis highlighted low air velocities behind the front face of the trailer for both vehicle configurations tested. This observation was supported by the wind tunnel tests because tuft movement was limited in these regions. These lower velocities may limit the replenishment of fresh air, and in terms of animal welfare, this aspect of the aerodynamics would appear to be negative. However, it is known that livestock are more comfortable when subjected to slower moving airflow. Indeed, high velocity jets may be likely to cause more discomfort and stress for the animals concerned. Obtaining the correct balance between ventilating livestock trailers adequately and maintaining comfortable conditions for the animals, is currently being assessed in greater detail.

The key for future livestock trailer design will be to modify the internal flow structure to provide a constant flow of air over the animals, at the optimum velocity for both animal comfort and effective heat extraction. Controlling the airflow is likely to be done using openings, vents and ducts strategically placed in the most appropriate locations. The fact that traditional livestock trailer design has been dictated by space requirements alone, neglecting aerodynamic considerations, does suggest that large gains could be made. However it should also be remembered that vehicles of this

type rely solely on passive ventilation, which is largely dependent on the ambient conditions. It follows that any proposed design should be effective over the widest range of possibilities, taking factors such as vehicle speed and different weather conditions into account.

CONCLUSION

The complementary nature of experimental and computational aerodynamic tools enabled a successful investigation into the ventilation characteristics of a generic livestock trailer to be undertaken. Good general agreement between the wind tunnel tests and the accompanying CFD analysis allowed the flow fields to be described accurately. The shape of the towing vehicle was found to have a major influence on the aerodynamic characteristics of livestock trailers, which in turn affected the ventilation inside the trailer. The results suggest that taller towing vehicles may be beneficial to the airflow inside the trailer, however this requires further investigation. An area of reduced air movement was identified behind the front face of the trailer and should be considered in future designs. Improved airflow characteristics were observed on the upper deck, driven by the rear vent.

ACKNOWLEDGEMENTS

The authors gratefully acknowledge the financial support of Defra under Grant Reference Number AW0933.

REFERENCES

[1] Hoxey R P; Kettlewell P J; Meehan A M; Baker C J; Yang X (1996). An investigation of the aerodynamic and ventilation characteristics of poultry transport vehicles. Part I: Full scale measurements. Journal of Agricultural Engineering Research, **65**, 77-83.

[2] Kettlewell P J; Hoxey R P; Hampson C J; Green N R; Veale B M; Mitchell M A. Design and operation of a prototype mechanical ventilation system for livestock transport vehicles. Journal of Agricultural Engineering Research, **79**, 429-439.

[3] Personal communication (2006).

[4] www.fluent.com.

[5] Sørensen D N; Nielsen P V (2003). Quality control of computational fluid dynamics in indoor environments. Indoor Air 2003, **13**, 2-17.

[6] Spalart P R, Allmaras S R (1994). A one-equation turbulence model for aerodynamic flows. La Recherche Aérospatiale, **1**, 5-21.

[7] Launder B E; Spalding D B (1974). The numerical computation of turbulent flow. Computer Methods in Applied Mechanics and Engineering, **3**, 269-289.

[8] Richardson L F (1927). The deferred approach to the limit. Transactions of the Royal Society London, Ser A, **226**, 229-361.

[9] Fluent User Guide.